Available online at www.sciencedirect.com
SCIENCE DIRECT®
International Journal of Heat and Mass Transfer 47 (2004) 2191–2203
International Journal of HEAT and MASS TRANSFER
www.elsevier.com/locate/ijhmt

Numerical simulation of nucleation, solidification, and microstructure formation in thermal spraying

H. Zhang [a,*], X.Y. Wang [b], L.L. Zheng [a], S. Sampath [b]

[a] Department of Mechanical Engineering, State University of New York at Stony Brook, Stony Brook, NY 11794-2300, USA
[b] Department of Materials Science and Engineering, State University of New York at Stony Brook, Stony Brook, NY 11794-2275, USA

Received 13 March 2003; received in revised form 22 November 2003

Abstract

A splat formation model has been developed based on the classic nucleation theory accounting for heterogeneous nucleation kinetic and crystal growth to predict the nucleation temperature and grain size distribution. The predicted grain size distribution has been compared with experimental data for molybdenum (Mo) splats on different substrates. The influence of the substrate material, interfacial thermal contact resistance, and wettability on the nucleation, grain size distribution, and rapid solidification process has been investigated. Based on scaling analysis, the nucleation delay and solidification times have been derived and compared with simulation results.

1. Introduction

Thermal spray processing is a well-established method combining the steps of melting, rapid quenching, and consolidation into a single step, and producing a variety of materials such as free-standing plasma-sprayed ceramic bodies, functionally graded materials, and fully and partially amorphous materials. The splat/coating formation is a highly non-equilibrium process leading to fine microstructure with features often of nanometer scale that is rather different from those in conventional materials. To establish the correlation between the coating quality and process parameters, it is important to develop a good understanding of the fundamental physical principles governing undercooling, nucleation, non-equilibrium solidification and microstructure formation.

In recent years, a number of research results have been published in nucleation and microstructure formation in thermal spraying. Jiang et al. [1–3] studied the microstructure formation of Mo splats on various substrate conditions to obtain the nucleation temperature [4]. Experiments were performed to obtain the grain size distribution of the final splats and correlate it to nucleation and solidification processes. Xu and Lavernia [5] developed a numerical model to predict the nucleation during thermal spraying. Their results confirmed that during the initial deposition stage, a second nucleation event may occur in the remaining liquid of impinging droplets. Two nucleation events generated intermixed small and large grains at the end of solidification. Chraska and King [6] reported on transmission electron microscopy (TEM) studies of microstructural features, e.g., grain size and cracks, and phase composition of the first layer (splat) on a smooth hot substrate. A rapid solidification model was also proposed to explain the observed narrow columnar grain microstructure of the yttria stabilized zirconia (YSZ) splat on a substrate. Based on the model, an estimate of liquid undercooling was calculated from the grain size. Friis et al. [7] studied the influence of particle in-flight characteristics on the coating microstructure. Experimental results showed that particle velocity and temperature, spraying angle and substrate temperature to be the most important parameters influencing the coating microstructure.

In this paper, a splat formation model including undercooling, nucleation, non-equilibrium solidification, and microstructure formation has been developed to predict the nucleation temperature and grain size

* Corresponding author. Tel.: +1-631-632-8492; fax: +1-631-632-8544.
E-mail address: hui.zhang@sunysb.edu (H. Zhang).

0017-9310/$ - see front matter © 2004 Elsevier Ltd. All rights reserved.
doi:10.1016/j.ijheatmasstransfer.2003.11.030

Nomenclature

a	constant
a_0	atom diameter
A_0	wetted area
b	splat thickness
Bi	Biot number, $Bi = h_c b/k_l$
C_p	specific heat
G_a	activation energy
G_c	nucleation barrier
h	Planck's constant
h_c	heat transfer coefficient
J	rate of nucleation
k	thermal conductivity
k_B	Boltzmann constant
L	latent heat of fusion
N_A	number of atoms
N_a	Avogadro's number
q''	heat flux
r	radial coordinate
R	thermal resistance
s	thickness of the deposited layer
s_R	rapid solidification fraction
St	Stefan number, $St = C_{pl}(T_p - T_f)/h_f$
t	time
T	temperature
V	velocity
y	vertical coordinate

Greek symbols

α	thermal diffusivity
μ_k	linear kinetic coefficient
ρ	density
θ	contact angle
σ	surface tension
σ_E	interface energy
Ω	molecular volume
Γ_Z	Zeldovih factor

Subscripts

B	bottom of the splat
c	contact area between splat and substrate
cr	critical
i	solidification interface
j	phase
J	rate of nucleation
k	kinetic
l	liquid
m	melting temperature
N	nucleation
ND	nucleation delay
p	splat
Re	recalesence
s	solidified layer
ss	top surface of the substrate
sub	substrate
T	thermal penetration
total	total solidification time

Superscripts

–	average
het	heterogeneous

distribution. The effects of contact angle, substrate temperature and splat radius on nucleation temperature and grain density are investigated. The grain size distribution has been predicted and compared with experimental data for molybdenum (Mo) splats on different substrates. Based on scaling analysis, the nucleation delay and total solidification time scales have been derived and compared with simulation results.

2. Mathematical models

2.1. Rapid solidification

Since the thickness of the splat is usually about two orders of magnitude smaller than the diameter of the splat [8,9], a one-dimensional heat conduction analysis is usually appropriate. Based on one-dimensional heat conduction, the problem can be described as follows

$$\rho_j C_{pj} \frac{\partial T_j}{\partial t} = \frac{\partial}{\partial y}\left(k_j \frac{\partial T_j}{\partial y}\right) \tag{1}$$

where the subscript j represents either solid or liquid phase in the splat, T is the temperature, t is the time, and y is the vertical coordinate normal to the substrate surface.

To consider the kinetic effects in rapid solidification of the splat, the interface temperature is assumed to be correlated to the interface velocity through the linear kinetics relationship [4],

$$V_i = \mu_k (T_m - T_i) \tag{2}$$

where μ_k is the linear kinetic coefficient, and T_m and T_i are the equilibrium freezing temperature and the actual interface temperature, respectively. The term, $T_m - T_i$, represents the undercooling. The energy balance condition at the solidification interface is expressed as follows:

$$\rho_s L \frac{ds}{dt} = k_s \left.\frac{\partial T_s}{\partial y}\right|_i - k_l \left.\frac{\partial T_l}{\partial y}\right|_i \tag{3}$$

where L is the latent heat of fusion and s is the thickness of the solidified layer.

An interfacial heat transfer coefficient, h_c, is introduced at the interface between the splat and substrate to quantify the thermal resistance due to a non-perfect contact between two surfaces. The interfacial boundary condition can be written as

$$k\frac{\partial T}{\partial y} = h_c(T_B - T_{ss}) \tag{4}$$

where T_B and T_{ss} are temperatures of the bottom surface of the splat and the top surface of the substrate, respectively. Note that the interfacial heat transfer coefficient is a complex function of the processing conditions and surface characteristics, and only limited quantitative data are available. In this paper, $h_c = 10^6$–10^8 W/m^2 K is used [8–10], and its value is assumed to remain unchanged during solidification. The substrate temperature far away from the splat, T_{sub}, is assumed to be constant. Adiabatic condition is applied to the top surface of the splat. The initial conditions are $T = T_p$ for the splat and $T = T_{sub}$ for the substrate.

2.2. Undercooling and nucleation

When a thin splat is located on a cold substrate, it will be greatly undercooled if the cooling rate is very high. Nucleation is mostly heterogeneous and starts on the substrate surface. The nucleated grains grow laterally to cover the substrate surface first, and then a stable set of narrow columnar grains continue to solidify with a planar solid/liquid interface and grow through the thickness of the splat in the direction of the heat flow [6]. The nucleation frequency at every time step can be calculated from the classical Becker–Doring/Turnbull–Fisher theory [11], assuming that the distribution of embryos can be relaxed to corresponding quasi-steady state within the time scale of the process. Following the conventional treatment of classical nucleation theory, the rate of nuclei formation in a molten splat can be expressed as [4]

$$J = N_A\frac{k_B T}{h}\Gamma_Z \exp\left(-\frac{\Delta G_a + \Delta G_C f(\theta)}{k_B T}\right) \tag{5}$$

where J is the rate of nucleation, N_A is the number of atoms located at the interface to the substrate, $\Gamma_Z = [\Delta G_C/(3\pi\kappa_B T)]^{1/2}$ is known as the Zeldovich factor, ΔG_a is the activation energy for interatomic diffusion in the liquid, ΔG_C is the nucleation barrier for homogeneous nucleation, κ_B is the Boltzmann constant, and h is the Planck's constant. The heterogeneous nucleation barrier, $\Delta G_C^{het} = \Delta G_C f(\theta)$, is a strong function of the melt undercooling and the solid/liquid interfacial energy σ_E, as well as the contact angle, θ, which represents the effect of the surface on nucleation.

$$\Delta G_C^{het} = \Delta G_C f(\theta) = \frac{16\pi}{3}\frac{\sigma_E^3 T_m^2}{[\rho_l L(T_m - T)]^2} f(\theta) \tag{6}$$

where the function, $f(\theta)$, represents the effect of surface on the lowering of activation energy required for nucleation and can be calculated using the following equation established from an energy balance at the interface:

$$f(\theta) = (2 + \cos\theta)(1 - \cos\theta)^2/4 \tag{7}$$

where θ is the contact angle between the nucleus and the catalytic surface. $\theta = 0$ corresponds to complete wetting with no nucleation barrier, while $\theta = 180°$ corresponds to no wetting between the splat and substrate, e.g., homogeneous nucleation.

The total number of atoms that are involved in the nucleation can be predicted as:

$$N_A = a_0 A_0 N_a/\Omega \tag{8}$$

where N_a is the Avogadro's number, Ω is the molecular volume, and A_0 is the available surface area for the splat melt in contact with the substrate. It can be calculated as $A_0 = A - A_n$, where A is the splat surface and A_n is the contact area of the nuclei, which can be calculated based on the radius of the nuclei in Eq. (11) and contact angle. In this model, we have assumed that all atoms, which are in contact with the substrate, will participate in nucleation. Such a classical nucleation model includes two important kinetic parameters, i.e., the solid/liquid interfacial energy and contact angle. The solid/liquid interfacial energy is a property of the sprayed materials, and only limited data are available in the open literature. The contact angle is a strong function of the physical and chemical properties of the substrate surface. In this study, it is treated as an adjustable parameter.

We assume that the number of nuclei formed during cooling and solidification may be approximated by a numerical integration of the nucleation frequency over time,

$$I = \int_{t_N}^{t} J(T,f)\,\mathrm{d}t \tag{9}$$

$$I_{k+1} = I_{k+1} + J(T,f)\Delta t \tag{10}$$

where $J(T,f)$ is the rate at which nuclei form on the surface of the substrate at temperature T. The initial condition for the numerical integration is $I = 0$ at the moment when the splat reaches the melting temperature ($T = T_m$). Since the value of I is assumed to be a continuous function, a nucleation event occurs every time when Eq. (9) produces a new integer value. The onset of solidification is marked at the time when the value of I reaches one, and this temperature is the nucleation temperature T_N.

2.3. Integrated model for grain density distribution

Once the nuclei form, they are assumed to grow as spheres whose radius, r_i, increases according to the following expression:

$$r_{i,k+1} = r_{i,k} + V_{i,k+1}\Delta t \tag{11}$$

where V_i denotes the interface velocity of the ith growing grain, which is approximated by Eq. (2), and Δt is the time step size. The computational procedures of calculating grain size distribution are listed as follows:

1. At a given time step $k+1$, Eqs. (1)–(4) are solved for the splat and substrate to obtain the temperature distributions in the splat and substrate.
2. Calculate the nucleation rate at time $k+1$, J, from Eq. (5) using the bottom temperature of the splat, T_B.
3. The number of nuclei at time $k+1$, I_{k+1}, is predicted by Eqs. (9) and (10). The nucleation begins if I_{k+1} is greater than or equal to 1. Nucleation temperature, T_N, is determined by the temperature when nucleation starts.
4. The radius of the nuclei, r_{k+1}, increases according to Eq. (11).
5. Check whether the splat surface in contact with the substrate is covered by grains or not.
6. If true, nucleation stops. Also the splat solidification takes place with a planar liquid/solid interface. Otherwise, go to the next time step and repeat steps (1) to (5).

3. Experimental observation

Thermal spray experiments were conducted to study single splat of molybdenum (Mo) on stainless steel and glass [2,3]. As shown in Fig. 1, the microstructure of typical coatings has a lamellar morphology and the columnar grain structure can be discerned within each layer. It suggests that nucleation and solidification from the bottom to the top of the splat in a columnar fashion. The average size of the columnar grains is about 0.4 μm for the first and also for the rest layers in Fig. 1(a). Fig. 1(b) shows the microstructure of a Mo splat on a glass substrate at a temperature of 480 °C. Experimental data show that the average size of the grains ranges from 4 to 6 μm. It should be noted that Fig. 1(b) shows only a small portion of the entire splat. It is evident that the grain size for Mo on stainless steel is smaller than that for Mo on glass. There are two possible mechanisms affecting grain distribution. One is the wettability described by the contact angle, which is a strong function of the substrate temperature and roughness, and the other one is the rate of solidification.

4. Numerical results and discussion

Numerical simulations were performed for molten Mo splats solidified on stainless steel or glass substrate with splat thickness of 2 and 1 μm, and diameter of 100 and 120 μm, respectively. The value roughly corresponds to the average splat size measured by a Zygo non-contact surface profiler—a scanning white-light interferometer. It is noted that the number of atoms involved in the surface heterogeneous nucleation is selected as that in contact with a smooth substrate surface with an area of 3×10^{-8} m^2 for Mo on stainless steel, which corresponds to the splat mentioned above. In the beginning of the calculation, a splat is assumed to have a uniform initial temperature, T_p. In addition, the initial substrate temperature is higher than the so-called "transition temperature" [12] and a continuous disk-like shape splat is considered for all cases investigated here. The physical properties used in calculations were listed in Table 1.

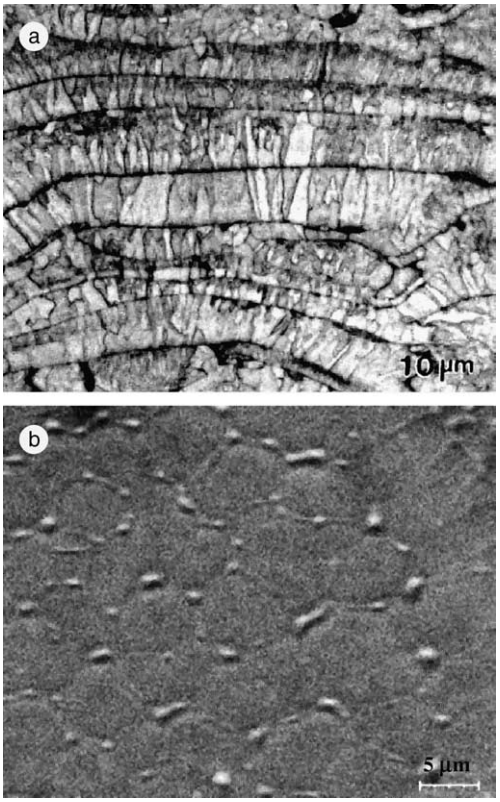

Fig. 1. (a) A SEM image showing lamellar structure of molybdenum coating on stainless steel substrate. (b) Optical image of molybdenum splats on glass substrate at temperature of 480 °C.

4.1. Analysis of solidification time

Based on the thermal network analysis, heat extraction from the substrate can be approximated as

$$q'' = \frac{T_m - T_{sub}}{R_k + R_s + R_c + R_{sub}} \tag{12}$$

Table 1
Thermophysical properties used in calculations [8,9]

Parameter	Mo	Steel	Glass
T_m, K	2883	1788	
L, J/kg	3.71×10^5	2.72×10^5	
k_l, W/m K	46	26	
k_s, W/m K	84	28	1.17
C_{pl}, J/kg K	570	866.67	
C_{ps}, J/kg K	339	690.82	900
ρ_l, kg/m^3	9350	7700	
ρ_s, kg/m^3	10,200	7850	2000
α_l, m^2/s	0.86×10^{-5}	3.9×10^{-6}	
α_s, m^2/s	2.43×10^{-5}	5.2×10^{-6}	6.5×10^{-7}
μ_k, m/s K	0.26	0.01	
ν, m^2/s	6.78×10^{-7}		
a_0, m	2.7×10^{-10}		
σ_E, J/m^2	0.33		
Ω, m^3/mol	1.04×10^{-5}		
ΔG_a, J/molecule	6.4×10^{-20}		

where R_k, R_s, R_c, and R_{sub} are thermal resistances of kinetic, solidified layer, thermal contact, and substrate, respectively, as shown in Fig. 2 and their values have been estimated in Table 2. Thermal resistance in the molten melt can be neglected since its thermal conductivity is usually large and thickness of the splat is usually very thin. In Table 2, V_i/q'' is estimated as $1/(\rho_s L)$, which is only true when thermal resistance in the melt is negligible. For Mo on stainless steel and glass, kinetics resistance can also be neglected. Furthermore, at the beginning of the solidification, the thermal resistance of the solidified layer is either zero or very small. The heat extraction from the substrate can then be simplified as

$$q'' = \frac{T_m - T_{sub}}{R_c + R_{sub}} = \frac{T_m - T_{ss}}{R_c} \tag{13}$$

where T_{ss} is the temperature on the top surface of the substrate, and can be estimated as

$$T_{ss} = T_{sub} + \frac{R_{sub}}{R_c + R_{sub}}(T_m - T_{sub}) \tag{14}$$

Noted that the above equation is only applicable at the beginning of the solidification process. At the later stage, the temperature on the top surface of the substrate can be approximated as

$$T_{ss} = T_{sub} + \frac{R_{sub}}{R_c + R_{sub}}(\overline{T}_B - T_{sub}) \tag{15}$$

where $\overline{T}_B$ is the average temperature on the bottom surface of the splat from the beginning of the contact to the time considered. By introducing a "critical time" as

$$t_{cr} = \left(\frac{k_{sub}}{h_c}\right)^2 \times \frac{1}{4\alpha_{sub}} \tag{16}$$

we can claim that the contact resistance will be the dominant when the solidification time is shorter than the critical time; otherwise the substrate thermal resistance is dominant. If the substrate thermal resistance is dominant, the Stefan solution should be employed to calculate the interface movement, e.g., $s = 2\lambda\sqrt{\alpha_s t}$. The interface elevation will, therefore, be proportional to $\sqrt{t}$, and the interface velocity will be reciprocal to the solidified fraction.

For Mo on stainless steel with $h_c = 10^6$ W/m^2 K or lower, the contact resistance will be the dominant for the entire solidification process. The interface elevation can then be estimated as

$$s = \frac{h_c(T_m - T_{ss})}{\rho_s L} t \tag{17}$$

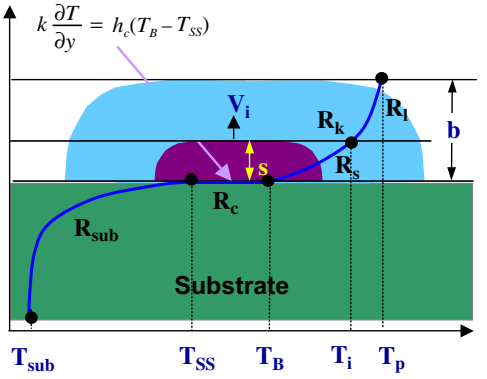

Fig. 2. Schematic of splat solidification.

Table 2
Thermal resistances of molten melt, kinetics, solidified layer, thermal contact, and substrate

Resistance	ΔT	Definition	Values
R_l	$T_p - T_m$	Assume small	~0
R_k	$T_m - T_i$	$V_i/\mu_k q'' \approx 1/(\rho_s L \mu_k)$	1.0×10^{-10}
R_s	$T_i - T_B$	$\delta_s/k_s \leqslant b/k_s$	2.4×10^{-8}
R_c	$T_B - T_{ss}$	$1/h_c$	10^{-6}–10^{-8}
R_{sub}	$T_{ss} - T_{sub}$	$\delta_{sub}/k_{sub} \approx \sqrt{4\alpha_{sub}t}/k_{sub}$	Mo on steel: $1.63\times10^{-4}\sqrt{t}$ Mo on glass: $1.38\times10^{-3}\sqrt{t}$

As a first order approximation, T_{ss} can be replaced by T_{sub}. Based on Eq. (17), the total solidification time can be simplified as

$$t_{total} = \frac{\rho_s L}{h_c(T_m - T_{ss})} b \tag{18}$$

where t_{total} should be smaller than t_{cr}.

In the case that the substrate thermal resistance is very small, e.g., $T_{ss} \approx T_{sub}$, and both kinetic and contact resistances are important, the interface evolution will be governed by the following equation (see Appendix A)

$$\left(\frac{1}{\mu_k} + \frac{\rho_s L}{h_c}\right) s + \frac{\rho_s L}{2k_s} s^2 = (T_m - T_{sub}) t \tag{19}$$

For rapid solidification, the interface velocity will begin with a large value of $V_i = \mu_k(T_m - T_N)$ and reduces to a smaller value of $V_i = \frac{h_c(T_m - T_{sub})}{\rho_s L}$.

4.2. Analysis of nucleation delay time

The Mo coating usually exhibits a columnar grain structure within each splat, indicating that solidification starts with surface nucleation, and followed by a planar interface growth. If the Biot number is large ($Bi > 1$), it is expected that the temperature profile in the melt is important. The splat will be cooled down at the bottom portion and the top portion of the splat may remain at the initial temperature. If at time $t = 0$, a splat with an initial temperature of T_p is suddenly exposed to a cold environment, with the heat flux of $q'' = h_c(T_B - T_{ss})$, the temperature at the bottom of the splat, T_B, can be calculated from [13]

$$\frac{T_B - T_{ss}}{T_p - T_{ss}} = e^{(h_c/k_l)^2 \alpha_l t} \operatorname{erfc}\left(\frac{h_c}{k_l}(\alpha_l t)^{1/2}\right) \tag{20}$$

It is reasonable to assume that nucleation begins as soon as the bottom temperature of the splat, T_B, reaches the nucleation temperature, T_N. If $(T_N - T_{ss})/(T_p - T_{ss}) = 0.8$ is assumed, $\frac{h_c}{k_l}(\alpha_l t)^{1/2} = 0.18$ can be obtained. The nucleation delay time for $Bi > 1$ can then be expressed as

$$t_{ND} = \frac{1}{\alpha_l}\left(\frac{0.18 k_l}{h_c}\right)^2 \tag{21}$$

The time scale of recalesence for $Bi > 1$ can also be evaluated as the time needed to heat up the undercooled portion of the melt to the equilibrium melting temperature. Through energy balance, the following formulation can be obtained

$$t_{Re} = \frac{\rho_l C_{pl}(T_m - T_N)\sqrt{4\alpha_l t_{ND}}}{\rho_s L \overline{V}_i} \approx \frac{2\rho_l C_{pl}(T_m - T_N)\sqrt{4\alpha_l t_{ND}}}{\rho_s L \mu_k (T_m - T_{sub})} \tag{22}$$

where the length scale, $\sqrt{4\alpha_l t_{ND}}$, is used to estimate the penetration depth during nucleation delay. The rest of the melt is assumed to remain at the initial temperature. In Eq. (22), $\overline{V}_i$ is the average velocity during recalesence. The interface velocity drops from a high value of $V_i = \mu_k(T_m - T_N)$ to a lower value of $V_i = \frac{h_c(T_m - T_{sub})}{\rho_s L}$. Half of the maximum value is used in our approximation.

If the Biot number is small ($Bi < 1$), it is expected that the splat will be cooled down uniformly. The nucleation delay time can then be estimated from

$$t_{ND} = \frac{\rho_l C_{pl}(T_p - T_N) b}{h_c(T_N - T_{sub})} \tag{23}$$

The time scale of recalesence for $Bi < 1$ can be estimated as the time needed to heat up the entire melt from nucleation temperature to the equilibrium melting temperature as

$$t_{Re} = \frac{2\rho_l C_{pl}(T_m - T_N) b}{\rho_s L \mu_k (T_m - T_{sub})} \tag{24}$$

Assuming that the splat is at a constant temperature in the case of $Bi < 1$, heat required for splat changing from nucleation temperature to the equilibrium melting temperature should be balanced with the latent heat release since only a small amount heat has been released from the substrate. The percentage of the solidified fraction that feels rapid solidification can be estimated as

$$s_R = \frac{C_{pl}(T_m - T_N) b}{L} \tag{25}$$

The percentage of the rapid solidified fraction is an important parameter related to the grain density distribution. It determines the thickness of the splat undergoing rapid solidification. It is expected that the grain density in rapid solidified portion will be finer and it will be coarser in the equilibrium solidification portion.

According to Trapaga et al. [14], the spreading time for a droplet on a flat surface can be approximated as

$$t_{spread} \approx DRe^{0.2}/V_p \tag{26}$$

For a 30 μm Mo droplet with a velocity of 150 m/s, the spreading time is about 1.16 μs from Eq. (26) after impinging on a flat substrate.

4.3. Nucleation delay and recalesence time

Fig. 3(a) shows the simulation results of the interface elevation for a Mo splat solidified on stainless steel substrate at $b = 2$ μm, $T_p = 3083$ K, $T_{sub} = 500$ K and $T_N = 2733$ K with different interfacial heat transfer coefficients. It is evident that thermal contact resistance is important if $h_c = 10^6$ W/m^2 K. Under this condition, the nucleation delay time from numerical simulation is

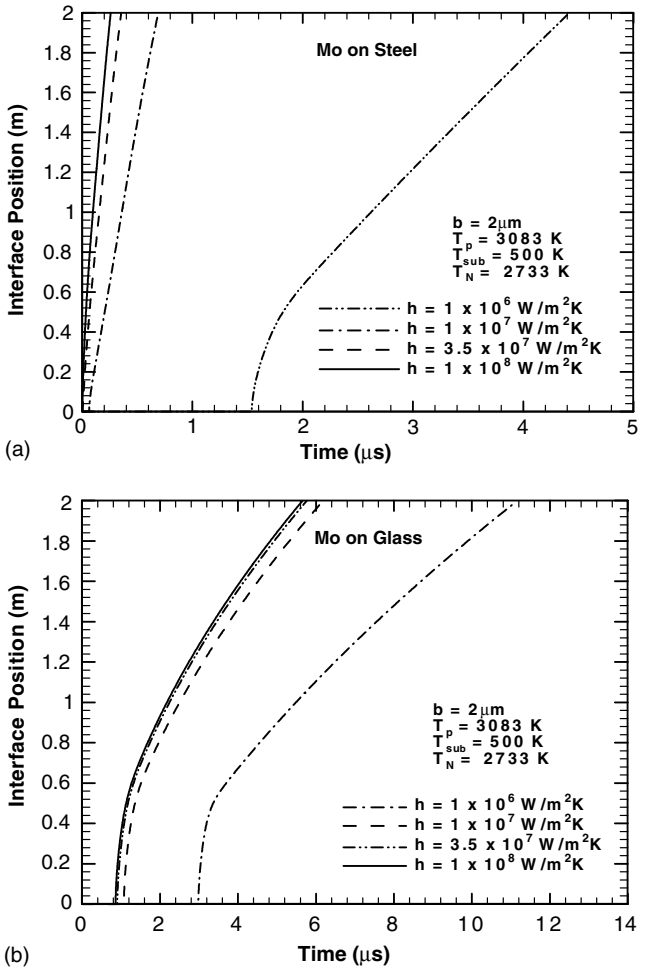

Fig. 3. Interface elevation as a function of time for molybdenum on stainless steel and glass.

about 1.54 μs, and the total solidification time is 4.4 μs. For a 30 μm Mo droplet impacting a stainless steel substrate, the analysis predicts $t_{\text{total}} = 3.2$ μs from Eq. (18) and $t_{\text{cr}} = 37.7$ μs from Eq. (16). The total solidification time of 3.2 μs is smaller than 4.4 μs obtained from numerical simulation. The error is primarily due to the nucleation delay and recalecense process. If the total solidification time is shorter than the critical time, the thermal contact resistance is important. The interface position can be expressed as $s = 0.63t$ from Eq. (17) for $h_{\text{c}} = 10^6$ W/m^2 K with $T_{\text{ss}} = T_{\text{sub}} = 500$ K. It is seen in Fig. 3(a) that a linear relationship between s and t exists for $t > 2$ μs or after recalesence is completed, and the slope of the linear line is about 0.6. Extending the linear line and crossing with the time axis, 0.8 μs is obtained. This is the difference between the theoretical and numerical predictions for the total solidification time. For a low Biot number, $Bi = h_{\text{c}}b/k_{\text{l}} \approx 0.043$ ($h_{\text{c}} = 10^6$ W/m^2 K and $b = 2$ μm), the time scales for nucleation delay and recalesence can be predicted as $t_{\text{ND}} = 1.57$ μs from Eq. (23), which is almost the same as the simulation result of 1.54 μs, and $t_{\text{Re}} = 0.0014$ μs from Eq. (24), which is slightly smaller than the simulation result, respectively. For a high interfacial heat transfer coefficient, the analytical solution of the nucleation delay time is also in good agreement with simulation results.

The spreading time, $t = 1.16$ μs, is smaller than the nucleation delay time for $h_{\text{c}} = 10^6$ W/m^2 K, $t = 1.57$ μs, and is larger than the nucleation delay time for $h_{\text{c}} = 10^7$ W/m^2 K, $t = 0.157$ μs. Noted that most numerical simulations in the open literature have neglected the time for undercooling and nucleation delay. The effects of solidification on the spreading process may be overpredicted. For Mo on glass substrate, as shown in Fig. 3(b), numerical results show that the behavior is very similar to that for Mo on stainless steel for $h_{\text{c}} = 10^6$ W/m^2 K. For Mo on glass, the thermal resistance of the substrate becomes a dominant resistance even in a short

time period; the thermal resistance is about 1.38×10^{-6} at $t = 1$ μs, the results for $h_c \geqslant 10^7$ W/m^2 K are therefore similar to each other since the process time is longer than 1 μs.

4.4. Solidified fraction and interface velocity

Fig. 4(a) and (b) shows the corresponding interface velocity variations as a function of solidified fraction for Mo on stainless steel and glass at different interfacial heat transfer coefficients. As expected, the interface velocity will begin with a large value of $V_i = \mu_k(T_m - T_N)$. When the interface penetrates further into the splat, the melt undercooling decreases, and the interface velocity changes to a smaller value of $V_i = \frac{h_c(T_m - T_{sub})}{\rho_s L}$. For the case of $h_c = 10^6$ W/m^2 K, numerical result shows that the interface velocity decreases from 39 m/s to steady state value of 0.60 m/s at the location in which the solidified fraction is 26%. The steady state value, 0.60 m/s, is smaller than 0.63 m/s from the analytical formulation. The good agreement between the analytical and simulation results demonstrates that the substrate heated up is limited in a short time period. The percentage of the splat that undergoes rapid solidification can be predicted as $s_R = 0.46$ μm from Eq. (25), which is 23% of the solidified fraction. Again the analytical formulation predicts the rapid solidified fraction accurately. It is expected that the grain density in this area will be finer and the portion above this area will be coarser due to the low rate of solidification.

For other three cases with $h_c > 10^6$ W/m^2 K in Fig. 4(a) and (b), the Biot numbers are no longer smaller than one. Temperature distribution in the melt becomes important. The bottom temperature of the splat drops very fast and reaches the nucleation temperature. The temperature of the upper portion of the splat may remain at the initial temperature due to the short penetration depth within a short nucleation delay time. Therefore, only a small amount of latent heat is needed to heat up the lower portion of the splat of which the temperature is lower than the equilibrium melting temperature. Using $h_c = 10^7$ W/m^2 K as an example, the nucleation delay time, and the thermal penetration

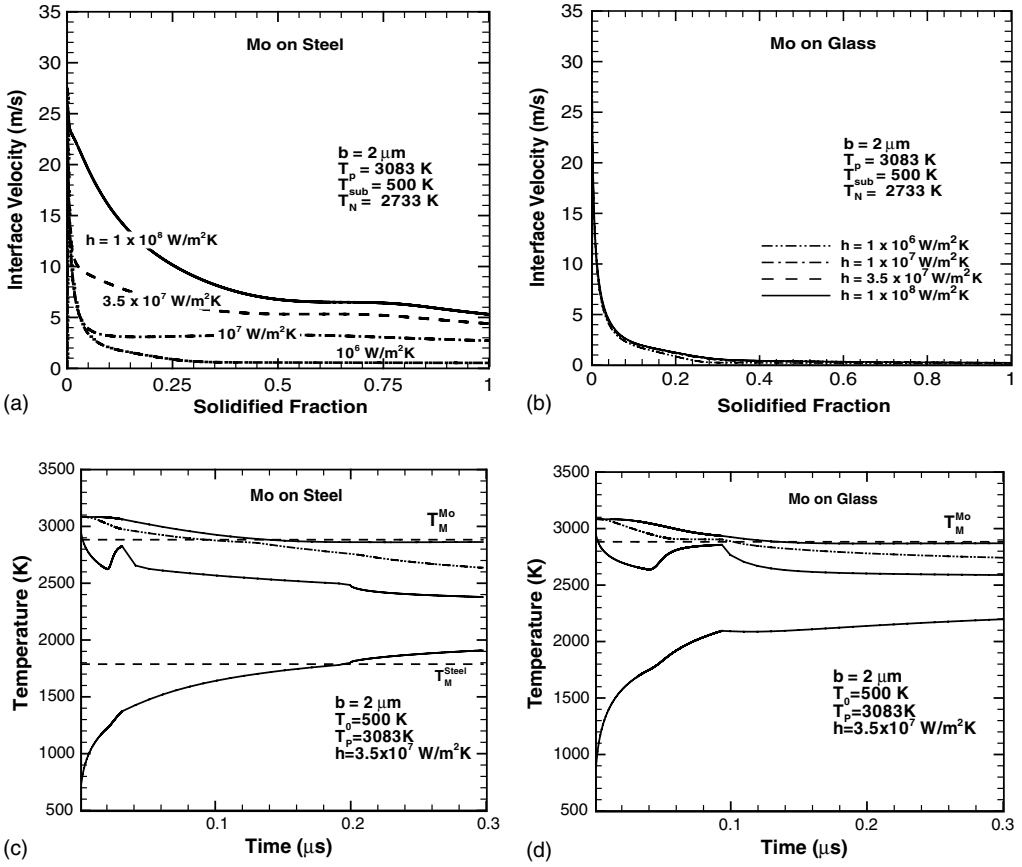

Fig. 4. Interface velocity as a function of solidified fraction for molybdenum on (a) stainless steel and (b) glass. Temperature variation in the splat for molybdenum on (c) stainless steel and (d) glass.

distance can be estimated as $t_{ND} = 8.0 \times 10^{-3}$ μs from Eq. (21) and $d_T \approx \sqrt{4\alpha_l t_{ND}} = 0.52$ μm, respectively. If the temperature profile in the splat is linear from the nucleation temperature at the bottom to the initial temperature at 0.52 μm depth into the splat, heat required to warm up the splat from a lower temperature to the equilibrium melting temperature should be balanced with the latent heat release. The percentage of the rapid solidified fraction can then be estimated as $s_R = C_{pl}(T_m - T_N)d_T/2L = 6\%$ which again agrees well with numerical results presented in Fig. 4(a). The same procedure can also be applied for other values of h_c. The steady state interface velocity is about 3 m/s for $h_c = 10^7$ W/m^2 K which is only half of the analytical result, $V_i = 6.3$ m/s from Eq. (17). This is due to a much higher temperature on the top surface of the substrate when the contact resistance is smaller than the substrate thermal resistance. A good estimation can be obtained from Eq. (14) for $T_{ss} = 1667$ K. Based on the same formulation, $V_i = \frac{h_c(T_m - T_{ss})}{\rho_s L} = 3.2$ m/s is predicted, which agrees with the numerical result. Further increasing the interfacial heat transfer coefficient, the Stefan solution should be used. The interface elevation will be proportional to $\sqrt{t}$, and the interface velocity should be reciprocal to the solidified fraction. The simulation result for $h_c = 10^8$ W/m^2 K confirms this behavior.

The interface temperature behaves like a mirror image of Fig. 4(a) and (b) due to the use of the linear kinetics relationship between the interface velocity and temperature. Again, undercooling for steady state case can be estimated from analytical formulations. Similar conclusions can be made for Mo on glass, as shown in Fig. 4(b).

4.5. Interface evolution in the splat

The Mo coating usually exhibits a columnar grain structure within each splat, indicating that solidification starts with surface nucleation and is followed by a planar interface growth. Fig. 4(c) and (d) shows the temperature profiles at three positions of the splat (bottom, middle, and top) and top surface of the substrate. As seen in the splat bottom temperature profile, the melt temperature next to the substrate decreases rapidly. After nucleation starts, the melt temperature at the bottom of the splat increases quickly. In Fig. 4(c), nucleation takes place at $t = 0.02$ μs. The top temperature of the substrate can be calculated as $T_{ss} = 2015$ K at $t = 0.3$ μs from Eq. (15) using $\overline{T}_B = 2500$ K. Both numerical and analytical results show that the substrate temperature is higher than the equilibrium melting temperature of stainless steel, e.g., substrate melting will happen for Mo on stainless steel. This phenomenon has also been confirmed in experiments (Zhang et al., 2001). Non-smooth profiles of the top surface temperature of the substrate and the bottom surface temperature of the splat are due to different thermophysical properties used in the solid and molten phases. The nucleation delay time is about 0.02 μs. In the case of $h_c = 3.5 \times 10^7$ W/m^2 K, the Biot number is 1.52, which is in the order of unity. The analytical formulation for either low or high Biot number is not applicable for this case. However, $t_{ND} = 0.045$ and 0.0065 μs can be obtained respectively if Eqs. (23) and (21) are employed. It is evident that the numerical result resides in between. The recalesence time of $t_{Re} = 0.0014$ μs is obtained from the analytical formulation, which is shorter than that from numerical simulation.

The temperature variation for Mo on glass is shown in Fig. 4(d). Temperature of the substrate surface increases quickly to 2000 K within 0.1 μs. The Mo nucleus appears at 0.04 μs, which is slightly longer than that for Mo on stainless steel. After nucleation, recalescence leads to a quick increase in the melt temperature. Consequently, the melt undercooling decreases. Compared with Mo on stainless steel, the recalescence curve is much wider than that for Mo on stainless steel. Although the thermal contact resistance for Mo on glass is assumed to be the same as that for Mo on stainless steel, the splat temperature in Mo on glass is more uniform because of a low thermal conductivity of glass. This is also the main reason that the grain size is coarser for Mo on glass than that for Mo on stainless steel.

4.6. Nucleation temperature

The nucleation temperature is a strong function of the contact angle for Mo on stainless steel, as shown in Fig. 5(a). The nucleation temperature decreases rapidly as the surface becomes ineffective to nucleation, i.e. when the contact angle increases. A good wetting condition (small contact angle) between the crystal nucleus and the substrate results in a decrease in ΔG_c. It will result in an increase of the rate of nucleus formation, which leads to a higher nucleation temperature. It is seen that the undercooling temperature more than 600 °C may be obtained for Mo and stainless steel. Noted that 700 °C undercooling has been estimated in Chraska and King [6] for YSZ on stainless steel. Although the contact angle has been widely used to describe the wettability between the splat and substrate, it is a lumped parameter related to not only material properties of molten splat, substrate and gas, but also roughness and other process parameters. Instead of establishing a relationship between the contact angle and those parameters, it may be beneficial to directly correlate the nucleation temperature with material and process parameters. The contact angle is, however, used in this paper due to the lack of necessary information.

The effect of the substrate temperature on nucleation temperature is indirect. It is believed that the nucleation

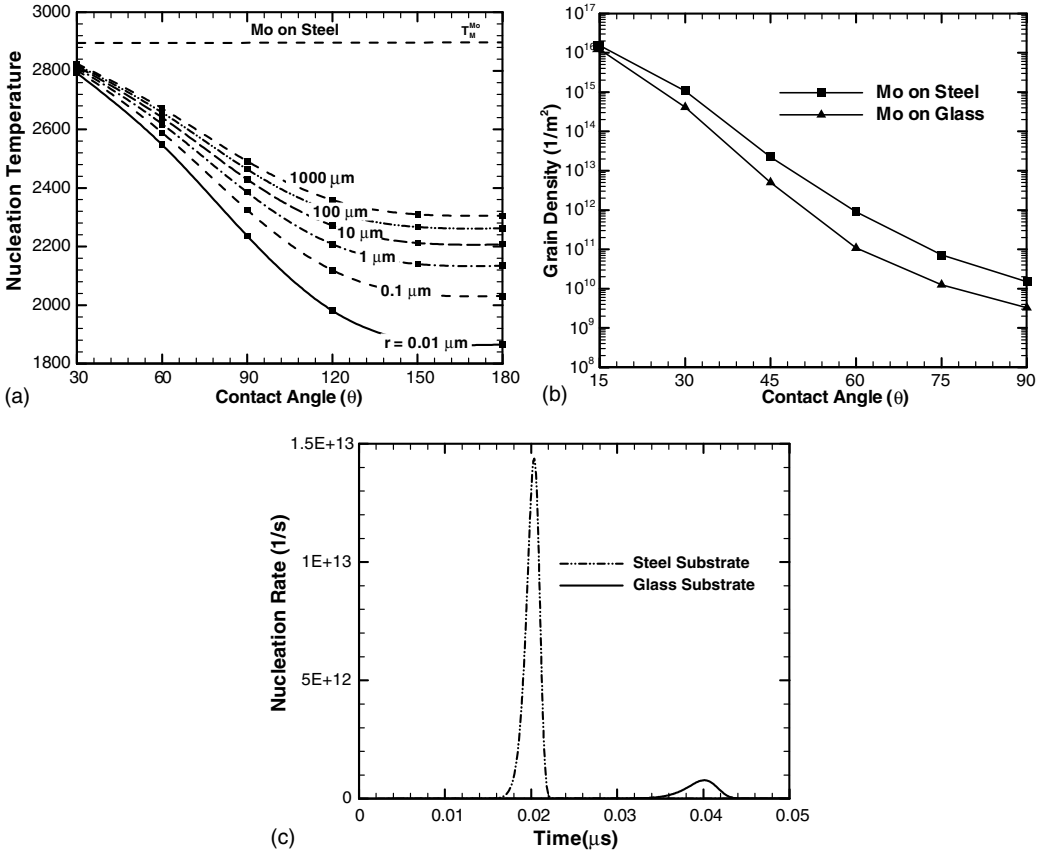

Fig. 5. (a) Nucleation temperature versus contact angle for molybdenum on stainless steel with different radius. (b) Grain density versus contact angle for molybdenum on stainless steel and glass. (c) Nucleation rates for molybdenum on stainless steel and glass at the temperature of 300 K, contact angle of 60° and splat thickness of 1 μm.

temperature will be a strong function of temperature in thermal spraying. For glass, it is believed that a high temperature makes the surface more hydrophobic by removing surface hydroxyl group [15]. For stainless steel, it is possible that a thin layer of oxide (<30 nm) appears on the substrate surface if the substrate temperature is higher than the "transition temperature" [2,3]. The existence of the oxide layer will change the wettability between the Mo droplet and stainless steel. Since only the contact angle appears in the formulation, all effects, such as substrate temperature, oxidation and surface chemistry are lumped into an "apparent contact angle".

The rate of heterogeneous nucleation assuming that the embryos forms on a foreign substrate is in quasi-steady equilibrium with the atoms from the parent phase in contact with the substrate. The melt area in contact with the substrate corresponds to the lower surface of the entire splat. If the latter is considered as a disk, the number of atoms can be directly linked to the radius of the splat. Fig. 5(a) shows the effects of the splat radius on the nucleation temperature. It seems that the nucleation temperature varies slightly with the splat radius, except for a high contact angle. When the foreign surface involved in the nucleation process is small and the wetting angle closes to 180°, the molten splat will experience a large undercooling leading to the formation of amorphous phase.

4.7. Grain density

Fig. 5(b) illustrates the grain density per square microns as a function of contact angle for Mo on stainless steel or glass. The grain density decreases as contact angle increases. The grain density and nucleation temperature exhibit the strong dependence on the contact angle. The contact angle in thermal spraying was usually estimated by comparing the predicted and measured grain density and average size [6]. In this paper, the contact angle is assumed to be 60° for Mo on both substrates. As shown in Fig. 5(b), the grain density is lower on glass substrate than that on steel substrate for

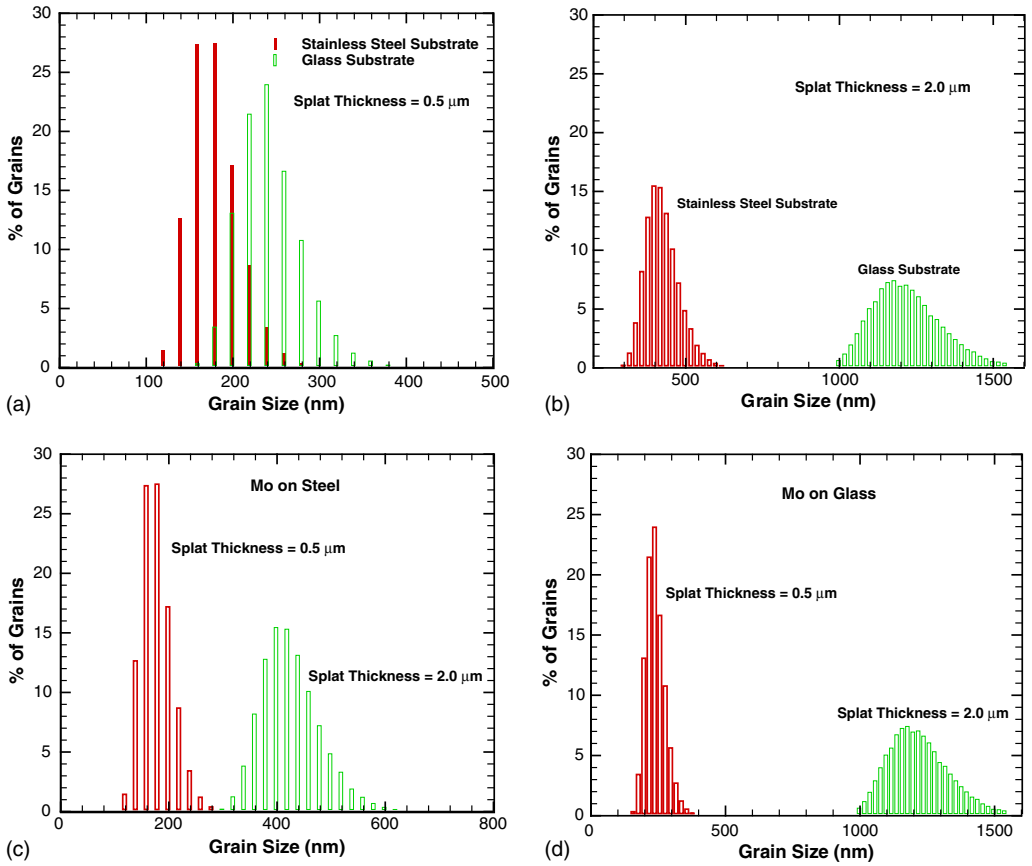

Fig. 6. Effect of grain size distribution on splat thickness: (a) 2 μm thickness and (b) 0.5 μm thickness; effect of grain size distribution on substrate materials (c) molybdenum on stainless steel and (d) molybdenum on glass.

the same contact angle. This is due to the low thermal conductivity of glass that results in a poor heat extraction during nucleation process.

As demonstrated in Fig. 6(a)–(d), the average grain size is much smaller for Mo on steel due to its high cooling rate. It should be noted that the size distribution is much scatter on the glass substrate and the average grain size is larger. Fig. 6(a) and (b) shows the effects of substrate materials on grain size distribution, and Fig. 6(c) and (d) shows the effects of splat thickness on grain size and distribution. It can be concluded that both material and geometry of the splat are important for the grain size distribution. It should be noted that the same contact angle of 60° is used for both Mo on stainless steel and Mo on glass. The differences between two cases are therefore mainly caused by splat cooling from the different substrates. Fig. 5(c) shows the evolution of the nucleation rate for Mo crystalline on stainless steel and glass at 300 K. It is revealed that the nucleation rate is higher and the nucleation occurs earlier on the stainless steel than that on glass due to different heat conductivities of two substrates. A higher heat extraction by stainless steel substrate results in a larger undercooling and higher nucleation rate.

5. Conclusions

A numerical model has been developed to study undercooling, heterogeneous nucleation, non-equilibrium solidification, and microstructure formation during thermal spraying. The influence of the substrate material, interfacial thermal contact resistance, and wettability on the nucleation, grain size distribution, and rapid solidification process has been investigated. The numerical model is able to predict the nucleation temperature, nucleation density, grain size distribution, nucleation rate, solidification velocity and thermal characteristics of rapid solidification. The numerical results are in good agreement with the experimental data in spite of the simplified assumptions.

The formulations of interface velocity, interface evolution, nucleation delay time and recalesence time have been driven from scaling analysis and theoretical results

are in good agreement with numerical predictions. The results reveal that the nucleation delay time may be longer than the spreading time if interfacial heat transfer coefficient is small. To accurately predict the influence of solidification on the spreading process, the undercooling and nucleation delay have to be considered, which have been neglected in the most open literature. Such assumptions may lead to an over-prediction on the role of solidification on the spreading process.

Numerical simulations showed that the splat next to substrate undergoes a significant degree of undercooling prior to nucleation, and the contact angle is the dominant factor to determine the nucleation temperature. Simulation results show that the nucleation temperature and grain size distribution strongly depends on contact angle. The nucleation temperature varies slightly with the splat radius if contact angle is not high. The substrate temperature will indirectly affect the nucleation temperature. Numerical results also show that the grain density of Mo is lower on glass substrate than that on steel substrate for the same contact angle. The nucleation rate is higher and nucleation occurs earlier on the steel substrate than that on glass substrate.

Acknowledgements

This work was supported by the National Science Foundation under award No. CTS-9876198 and MRSEC program under award No. DMR-0080021. Technical discussions with Dr. G.X. Wang of Akron University were very helpful and acknowledged.

Appendix A

If heat transfer contribution in the molten melt can be neglected, the movement of the solidification front will be governed by

$$V_i = \mu_k (T_m - T_i) \tag{A.1}$$

$$\rho_s L V_i = k_s \left.\frac{\partial T_s}{\partial y}\right|_i \tag{A.2}$$

and

$$k_s \left.\frac{\partial T_s}{\partial y}\right|_i = h_c (T_B - T_{ss}) \tag{A.3}$$

If the substrate thermal resistance is very small and temperature distribution in the solidified layer is approximated as a linear profile. The following relationship can be deduced from Eq. (A.3),

$$T_B - T_{sub} = \frac{T_i - T_{sub}}{1 + \frac{h_c}{k_s} \cdot s} \tag{A.4}$$

Combining Eqs. (A.2) and (A.4), we obtain

$$\frac{ds}{dt} = \frac{T_i - T_{sub}}{\frac{\rho_s L}{h_c} + \frac{\rho_s L}{k_s} s} \tag{A.5}$$

Substituting Eq. (A.5) into Eq. (A.1), the interface temperature can be deduced as,

$$T_i - T_{sub} = \frac{\frac{\rho_s L}{h_c} + \frac{\rho_s L}{k_s} s}{\frac{1}{\mu_k} + \frac{\rho_s L}{h_c} + \frac{\rho_s L}{k_s} s} (T_m - T_{sub}) \tag{A.6}$$

and the interface velocity can then be calculated as follows

$$V_i = \frac{ds}{dt} = \frac{T_m - T_{sub}}{\frac{1}{\mu_k} + \frac{\rho_s L}{h_c} + \frac{\rho_s L}{k_s} s} \tag{A.7}$$

The thickness of the solidified layer can be obtained by integrating Eq. (A.7) as

$$\left(\frac{1}{\mu_k} + \frac{\rho_s L}{h_c}\right) s + \frac{\rho_s L}{2 k_s} s^2 = (T_m - T_{sub}) t \tag{A.8}$$

References

[1] X.Y. Jiang, Deposit Formation Dynamics and Microstructure Development during Thermal Spraying, PhD thesis, State University of New York at Stony Brook, Stony Brook, NY, 2000.

[2] X.Y. Jiang, J. Matejicek, S. Sampath, Substrate temperature effects on the splat formation, microstructure development and properties of plasma sprayed coatings. Part II: Case study for molybdenum, Mater. Sci. Eng. A 272 (1999) 189–198.

[3] X.Y. Jiang, H. Herman, S. Sampath, Grain morphology of plasma sprayed molybdenum splats on glass substrate, Mater. Sci. Eng. A 299 (2001) 235–240.

[4] C.G. Levi, R. Mehrabian, Heat flow during rapid solidification of undercooled metal droplets, Metall. Trans. A 19 (1982) 699–708.

[5] Q. Xu, E.J. Lavernia, Influence of nucleation and growth phenomena on microstructural evolution during droplet-based deposition, Acta Mater. 49 (2001) 3849–3861.

[6] T. Chraska, A.H. King, Transmission electron microscopy study of rapid solidification of plasma sprayed zirconia. Part I: First splat solidification, Thin Solid Films 397 (2001) 30–39.

[7] M. Friis, C. Persson, J. Wigren, Influence of particle in-flight characteristics on the microstructure of atomspheric plasma sprayed yttria stabilized ZrO_2, Surf. Coat. Technol. 141 (2001) 115–127.

[8] H. Zhang, X.Y. Wang, L.L. Zheng, X.Y. Jiang, Studies of splat morphology and rapid solidification during thermal spraying, Int. J. Heat Mass Transfer 44 (2001) 4579–4592.

[9] X.Y. Wang, H. Zhang, L.L. Zheng, S. Sampath, A micro/macro integrated model for melt flow and non-equilibrium solidification for thermal spraying, Int. J. Heat Mass Transfer 45 (2002) 2289–2301.

[10] G.X. Wang, E.F. Matthys, Experimental investigation of interfacial thermal conductance for molten metal solidification on a substrate, J. Heat Transfer 118 (1996) 157–163.
[11] D. Turnbull, J.C. Fisher, Rate of nucleation in condensed systems, J. Chem. Phys. Phys. 17 (1949) 71–73.
[12] M. Fukumoto, E. Nishioka, T. Matsubara, Flattening and solidification behavior of a metal droplet on a flat substrate surface held at various temperatures, Surf. Coat. Technol. 120–121 (1999) 131–137.
[13] A.F. Mills, Heat Transfer, second ed., Prentice Hall, New Jersay, 1999, pp. 167–187.
[14] G. Trapaga, E.F. Matthys, J.J. Valencia, J. Szekely, Fluid flow, heat transfer, and solidification of molten metal droplets impinging on substrates: comparison of numerical and experimental results, Metall. Trans. 23B (1992) 701–718.
[15] J. Hautman, M.L. Klein, Micorscopic wetting phenomena, Phys. Rev. Lett. 67 (1991) 1763–1766.